### Trans-Basin Influence of Southwest Tropical Indian Ocean Warming during Early Boreal Summer

ZESHENG CHEN, a,b ZHENNING LI, YAN DU, a,b,d ZHIPING WEN, RENGUANG WU, AND SHANG-PING XIE

<sup>a</sup> State Key Laboratory of Tropical Oceanography, South China Sea Institute of Oceanology, Chinese Academy of Sciences, Guangzhou, China

<sup>b</sup> Southern Marine Science and Engineering Guangdong Laboratory, Guangzhou, China

<sup>c</sup> Division of Environment and Sustainability, Hong Kong University of Science and Technology, Hong Kong, China <sup>d</sup> University of Chinese Academy of Sciences, Beijing, China

<sup>e</sup> Department of Atmospheric and Oceanic Sciences/Institute of Atmospheric Sciences, Fudan University, Shanghai, China <sup>f</sup> School of Earth Sciences, Zhejiang University, Hangzhou, China <sup>g</sup> Scripps Institution of Oceanography, University of California, San Diego, California

(Manuscript received 2 December 2020, in final form 26 July 2021)

ABSTRACT: This study examines the climate response to a sea surface temperature (SST) warming imposed over the southwest tropical Indian Ocean (TIO) in a coupled ocean-atmosphere model. The results indicate that the southwest TIO SST warming can remotely modulate the atmospheric circulation over the western North Pacific Ocean (WNP) via interbasin air-sea interaction during early boreal summer. The southwest TIO SST warming induces a "C shaped" wind response with northeasterly and northwesterly anomalies over the north and south TIO, respectively. The northeasterly wind anomalies contribute to the north TIO SST warming via a positive wind-evaporation-SST (WES) feedback after the Asian summer monsoon onset. In June, the easterly wind response extends into the WNP, inducing an SST cooling by WES feedback on the background trade winds. Both the north TIO SST warming and the WNP SST cooling contribute to an anomalous anticyclonic circulation (AAC) over the WNP. The north TIO SST warming, WNP SST cooling, and AAC constitute an interbasin coupled mode called the Indo-western Pacific Ocean capacitor (IPOC), and the southwest TIO SST warming could be a trigger for IPOC. While the summertime southwest TIO SST warming is often associated with antecedent El Niño, the warming in 2020 seems to be related to extreme Indian Ocean dipole during the autumn of 2019. The strong southwest TIO SST warming seems to partly explain the strong summer AAC of 2020 over the WNP even without a strong antecedent El Niño.

KEYWORDS: Anticyclones; Atmosphere-ocean interaction; El Niño; Flood events; Monsoons

#### 1. Introduction

El Niño-Southern Oscillation (ENSO) is a dominant air-sea coupled mode in the equatorial Pacific that has profound impacts on the global climate. Over the TIO, SST warming follows the positive phase of ENSO (i.e., the El Niño) at a lag of one season (Klein et al. 1999; Chiang and Sobel 2002; Lau and Nath 2003; Alexander et al. 2002). ENSO peaks in boreal winter (November-January). When ENSO-related SST anomalies decay in the equatorial Pacific, the TIO SST anomalies remain robust with profound impacts on Indo-Pacific climate (Annamalai et al. 2005; Yang et al. 2007; Xie et al. 2009; Du et al. 2011; Wu et al. 2010; Chowdary et al. 2011; Hu et al. 2011; Zhan et al. 2011; Qu and Huang 2012; Cao et al. 2013; He et al. 2015; Chen et al. 2016, 2018).

The thermocline in the equatorial Indian Ocean is flat and deep due to the annual mean weak westerly winds, limiting the effect of thermocline displacements on SST variability (Schott et al. 2009). El Niño-induced surface heat flux change explains most of the TIO SST warming except for the warming over the southwest TIO (Klein et al. 1999). In the southwest TIO where the mean thermocline is shallow, the thermocline feedback on SST is strong. During a positive Indian Ocean dipole or an El Niño event, anticyclonic surface wind stress curl anomalies

Corresponding author: Yan Du, duyan@scsio.ac.cn

over the south TIO force downwelling oceanic Rossby waves propagating westward. The deepened thermocline causes SST to rise (e.g., Murtugudde et al. 2000; Behera and Yamagata 2001; Xie et al. 2002; Huang and Kinter 2002).

The TIO warming in the El Niño decay phase features considerable regional variations. The southwest TIO warming persists into boreal summer next year, enhancing deep convection in situ. The intensified convection induces a "C shaped" wind anomaly pattern with anomalous northeasterly winds north and northwesterly winds south of the equator (Wu et al. 2008; Wu and Yeh 2010; Izumo et al. 2008).

After the Asian monsoon onset (in May), the mean low-level winds change from northeasterly to southwesterly. The climatological SST cools down in the western Arabian Sea, mainly due to the southwesterly jet-induced Somalia-Oman coastal upwelling (Findlater 1969; Murtugudde et al. 2007). So, the northeasterly wind anomalies along the Somalia-Oman coasts anchored by the southwest TIO warming decrease offshore Ekman ocean transport, coastal upwelling, and latent heat flux, and thus warm the mixed layer in the western Arabian Sea (Izumo et al. 2008). Besides, the northeasterly wind anomalies on the northern flank of the C-shaped wind anomaly pattern weaken wind speed and surface latent heat flux loss in the north TIO, and thus contribute to the second SST warming via positive wind-evaporation-SST (WES) feedback (Xie and Philander 1994; Xie 1996; Du et al. 2009).

# The wind Response to Southwest TIO Warming in CAM4

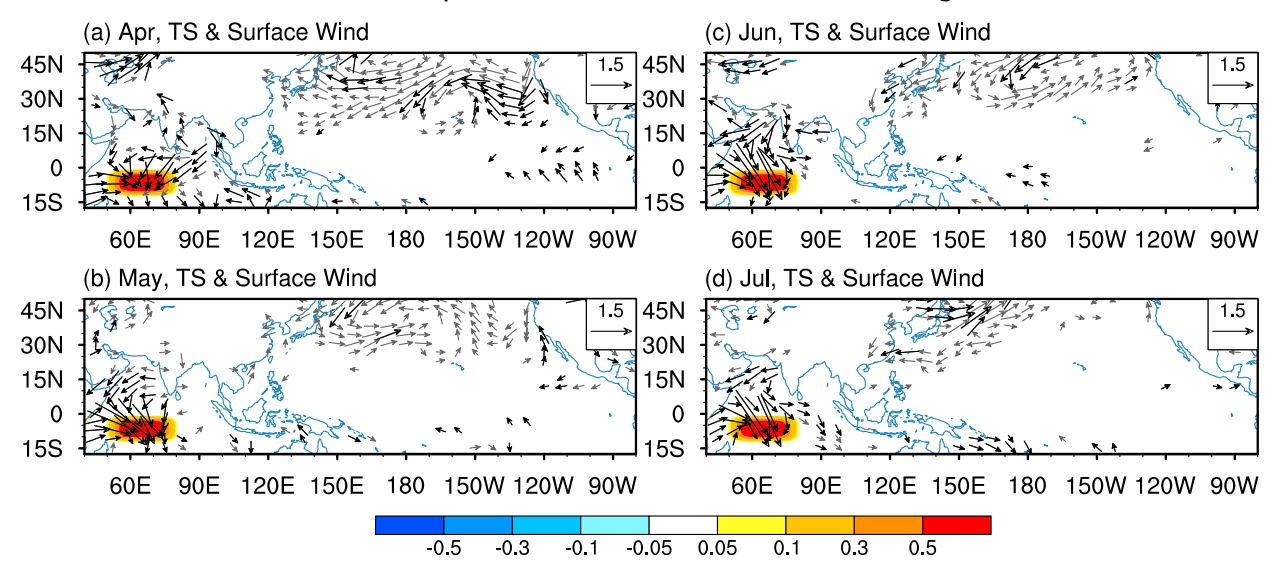


FIG. 1. The impacts of southwest TIO warming in an AGCM experiment designed in Chen et al. (2019). The shading is the ideal SST anomalies used to force CAM4 and in our current CESM sensitivity experiment. The center of the southwest TIO SST warming is located at 6.5°S and 65°E, with its maximum warming reaching 0.8°C, and the area-mean amplitude of southwest TIO SST warming is about 0.4°C.

A recent study found that the southeast TIO SST warming always follows the southwest TIO SST warming during strong El Niño events, and oceanic wave reflection plays a role in linking the southwest and southeast TIO warming (Chen et al. 2019). The westward propagation of oceanic downwelling Rossby waves contributes to the SST warming in the southwest TIO. The Rossby waves arrive at the western boundary and are reflected as oceanic Kelvin waves. The downwelling Kelvin waves propagate along the equator, deepening the thermocline off the Sumatra and Java Islands and suppressing the monsoon-induced coastal upwelling, setting a favorable condition for the southeast TIO warming (Chen et al. 2019).

South TIO variability can affect the north TIO (e.g., Wu et al. 2008; Chen et al. 2018). It is still unclear whether its influence extends all the way to climate over East Asia. To explore the climatic impact of the southwest TIO warming, Chen et al. (2019) conducted two numerical experiments using Community Atmosphere Model, version 4 (CAM4), at a horizontal resolution equivalent to  $0.9^{\circ} \times 1.25^{\circ}$ . The control run was forced by the climatological mean annual cycle of SSTs. In the sensitivity run, idealized southwest TIO SST anomalies (Fig. 1) were added to the control-run-used SSTs to force the model. Each run was a 35vr continuous simulation. The ensemble mean difference between these two experiments indicates the direct atmospheric response to the southwest TIO warming (Chen et al. 2019). Figure 1 shows the low-level wind (i.e., 925-hPa wind) response to southwest TIO warming in an atmospheric general circulation model (AGCM) experiment as in Chen et al. (2019). The AGCM result suggested that the direct effect of southwest TIO warming does not extend far enough to modulate the atmospheric circulation over the western North Pacific (WNP). This does not rule out a southwest TIO effect on the WNP through the air–sea interaction processes. Indeed, observational analysis indicates that southwest TIO warming is followed by anomalous easterly winds across the north Indian Ocean and WNP as part of the anticyclonic circulation over WNP (Fig. 2). The apparent contradiction between the observational analysis and AGCM simulation motivates us to reexamine the role of southwest TIO warming in modulating the atmospheric circulation over the WNP using the Community Earth System Model, version 1.0.4 (CESM1.0.4). The coupled modeling results show that the southwest TIO warming has a trans-basin influence on the WNP. Specifically, the southwest TIO warming induces SST cooling east of the Philippine islands through interbasin air–sea interaction, which, in turn, induces the anticyclonic circulation over the WNP.

The rest of the paper is organized as follows. Section 2 describes the data and methods used in this study. Section 3 evaluates the model performance and examines the trans-basin response to southwest TIO SST warming in CESM simulations. Section 4 discusses the role of southwest TIO SST warming in contributing to heavy rainfall in southern China in June 2020. Section 5 presents the summary and conclusions.

#### 2. Data and model experiments

### a. Data

In this study, we use monthly National Oceanic and Atmospheric Administration (NOAA) Optimum Interpolation SST V2 (OISST, Reynolds et al. 2002) on a 1.0° × 1.0° global grid (https://psl.noaa.gov/data/gridded/data.noaa.oisst.v2.html); monthly precipitation data on a 2.5° × 2.5° grid from the Global Precipitation Climatology Project (GPCP; Adler et al. 2003)

# Regressions with Normalized SWTIO SST Index

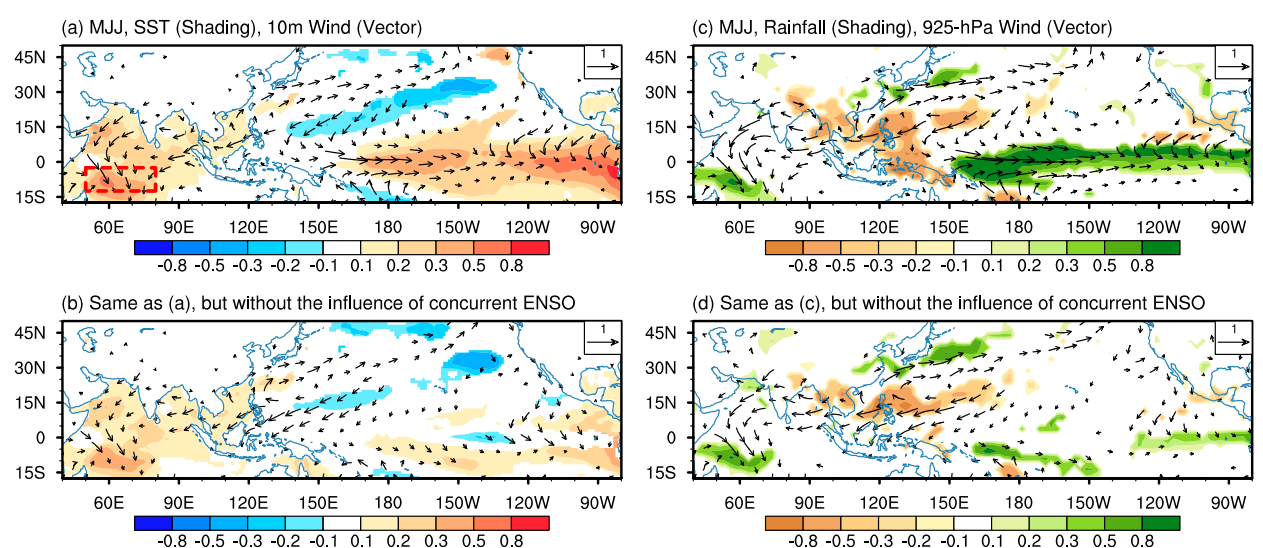


FIG. 2. SST, rainfall, and surface wind regressed onto May–July (MJJ) southwest TIO SST index. Only the regressed anomalies that are significant at the 95% confidence level according to a two-tailed Student's *t* test are plotted. The southwest TIO SST index is defined as the SST anomalies averaged in the region inside the red-outlined box in (a).

(https://psl.noaa.gov/data/gridded/data.gpcp.html); and monthly zonal and meridional wind from the fifth generation of the European Centre for Medium-Range Weather Forecasts (ECMWF) atmospheric reanalysis (ERA5; Hersbach et al. 2020). The ERA5 data were produced using 4D-Var data assimilation and cover Earth on a 30-km grid, with 137 hybrid sigma/pressure levels from the surface up to a height of 80 km. Here, we use the interpolated version of ERA5 data that has a  $1.0^{\circ} \times 1.0^{\circ}$  horizontal resolution, with 37 pressure levels and one surface level (https://climate.copernicus.eu/climate-reanalysis). All datasets are available from January 1982 to September 2020. The monthly anomalies are calculated by subtracting the annual cycle and removing the linear trend. The confidence level of correlation and regression analysis is evaluated by two-tailed Student's t test. The Niño-3.4 SST index is defined as the SST anomalies averaged in the Niño-3.4 region (i.e., 5°S-5°N, 170°-120°W). The southwest TIO SST index is defined as the SST anomalies averaged in the southwest TIO (i.e., 12.5°-2.5°S, 50°-80°E). The Indian Ocean dipole mode index (DMI; Saji et al. 1999) is defined as the SST anomalies difference between the western  $(10^{\circ}\text{S}-10^{\circ}\text{N}, 50^{\circ}-70^{\circ}\text{E})$  and eastern  $(0^{\circ}-10^{\circ}\text{S}, 90^{\circ}-110^{\circ}\text{E})$ parts of the Indian Ocean.

### b. Model experiments

The CESM, version 1, released by the National Center for Atmospheric Research (NCAR) is used in this study. Using the "B2000" component setting, the CESM is a fully coupled global climate model, with interacting components of the atmosphere (CAM4), ocean (POP2), land (CLM4), and sea ice (CICE4), equivalent to using the Community Climate System Model, version 4 (CCSM4, Gent et al. 2011). The values of solar forcing, carbon dioxide, aerosol, and ozone concentration are fixed at their levels of the year 2000. In the

coupled run, the atmosphere model was run at a  $1.9^{\circ} \times 2.5^{\circ}$  horizontal resolution and 26 vertical levels, the ocean model was run at an approximate 1° horizontal resolution on displaced dipole coordinates and 60 levels.

We implemented a control run (referred to as the CTRL run) with 300-yr integration. The model reached a quasi-equilibrium after 250-yr spinup, and we choose the last 50-yr output for analysis. To isolate the impacts of southwest TIO warming, a sensitivity experiment is conducted, branching from the CTRL run on 1 January of simulated year 251. The sensitivity experiment is 50 years long, where we prescribed the SST in the southwest TIO. The model is fully coupled in the rest of the globe. We called this sensitivity experiment the southwest TIO pacemaker experiment (SWTIO-P run). The prescribed SST forcing in the southwest TIO is constructed by adding an idealized SST anomaly pattern to the climatological SST derived from the last 50-yr CTRL run output. Following Chen et al. (2019), the SST anomaly pattern is time-invariant from February to September, with its maximum intensity reaching 0.8°C at 6.5°S, 65°E. The area average SST anomaly in the southwest TIO (2.5°-12.5°S, 50°-80°E) is about 0.4°C (Fig. 1). A two-tailed Student's t test is used to evaluate the confidence level of the differences between sensitivity run and CTRL run.

### 3. Numerical model results

### a. Model performance

We compared the climatology of simulated rainfall, zonal wind at 925 hPa, and SST in the CESM control run with observations. Figure 3 illustrates the Taylor diagram (Taylor 2001) displaying a statistical comparison of CESM control run with observations in 17.5°S–40°N, 40°E–80°W. For SST, the

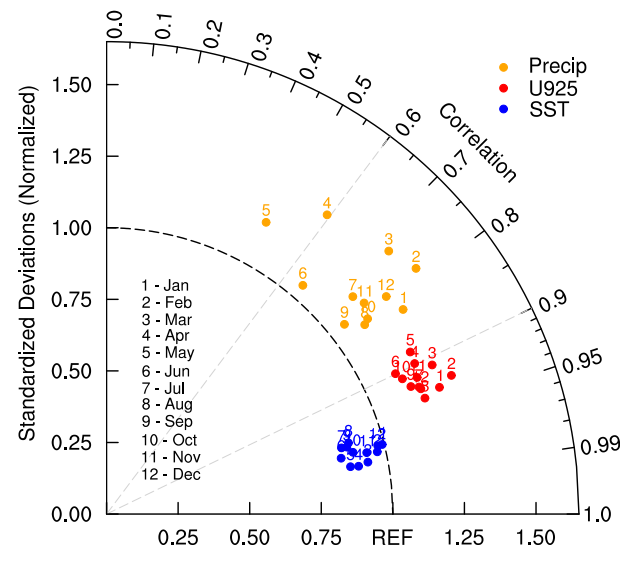


FIG. 3. Taylor diagram displaying a statistical comparison of the CESM control run with observations. Here, we selected three variables (i.e., rainfall, zonal wind at 925 hPa, and SST), and compared the simulated spatial pattern of their climatology for every month with observations.

spatial correlation between the simulation and observations is high (0.95 or above). The simulated low-level zonal wind (i.e., zonal wind at 925 hPa) also resemble the observations, with a spatial correlation of around 0.9. For rainfall, the spatial correlation varies from around 0.5 in May to 0.85 in January. In comparison with observations, the CESM simulation underestimates the spatial variation of SST but overestimates those of rainfall and low-level zonal wind. Overall, the CESM control run can reasonably capture the major spatial features of climatology for every month.

Figure 4 shows the simulated mean SST, low-level wind, and rainfall in June. The CESM control run can reasonably capture the main observational spatial features of the June climate. The ITCZ over the tropical Indian Ocean and Pacific, the monsoon circulation with westerly winds blowing in the north Indian Ocean and the South China Sea (SCS), and the Indo-Pacific warm pool resemble the observations (Fig. 4). There are some deficiencies in the CESM control run. For example, the intensity of the mei-yu/baiu/changma rainband is weaker than observations, and the rainfall intensity over the ITCZ region is stronger than observations. The spatial correlation between the simulated rainfall and GPCP precipitation in June is 0.65 (Fig. 3). Note that the wind response in the CESM seems to be more reliable when compared with the rainfall response (Figs. 3 and 4).

Figures 5a and 5b compare the seasonal evolution of surface wind (i.e., 10-m wind) averaged over 10°-20°N for observations and the CESM CTRL run. In observations, the monsoonal southwesterly winds are well established in the north Indian Ocean around May and gradually extend eastward into the SCS and WNP (Fig. 5a). The CESM CTRL run well simulates the seasonal migration of the summer monsoon and the seasonal transition of easterly wind into the westerly wind over the WNP (Fig. 5b). We also compared the composite result of six strong southwest TIO warming events during early boreal summer in the CESM CTRL run and observations. The CTRL run is capable of simulating the key processes related to the southwest TIO SST warming in the observations, such as the "C-shaped" wind response in the TIO and anticyclonic wind response in the WNP (figures not shown).

#### b. Trans-basin influence of the southwest TIO warming

The impacts of the southwest TIO warming can be evaluated by analyzing the differences between the SWTIO-P and CTRL runs. Figure 6 shows the simulated rainfall and low-level wind differences between SWTIO-P run and CTRL run. In response

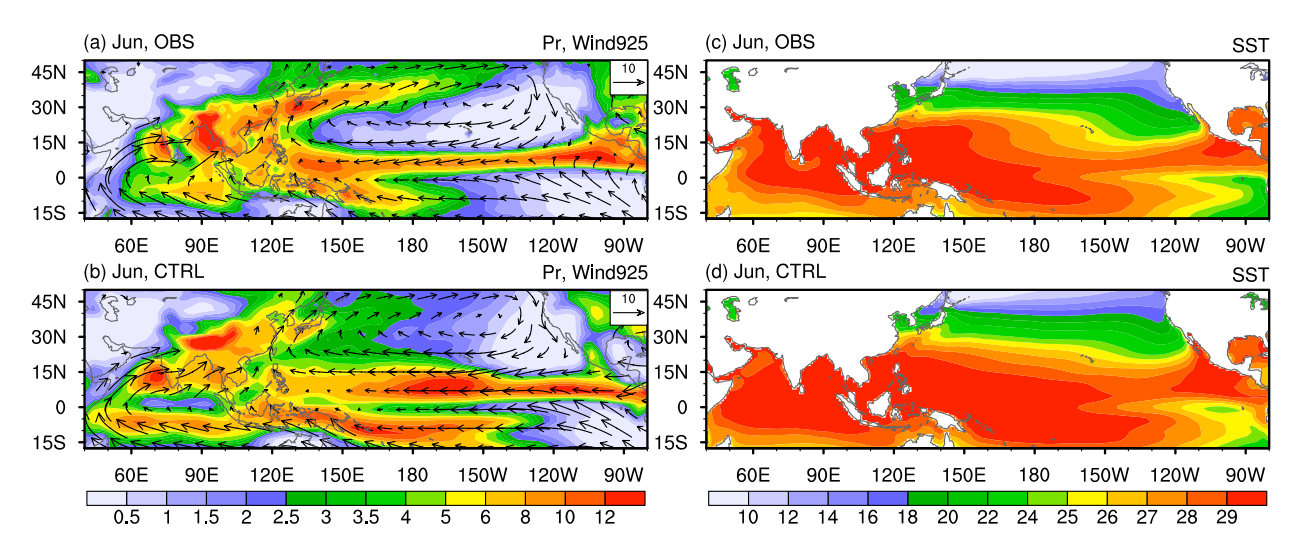
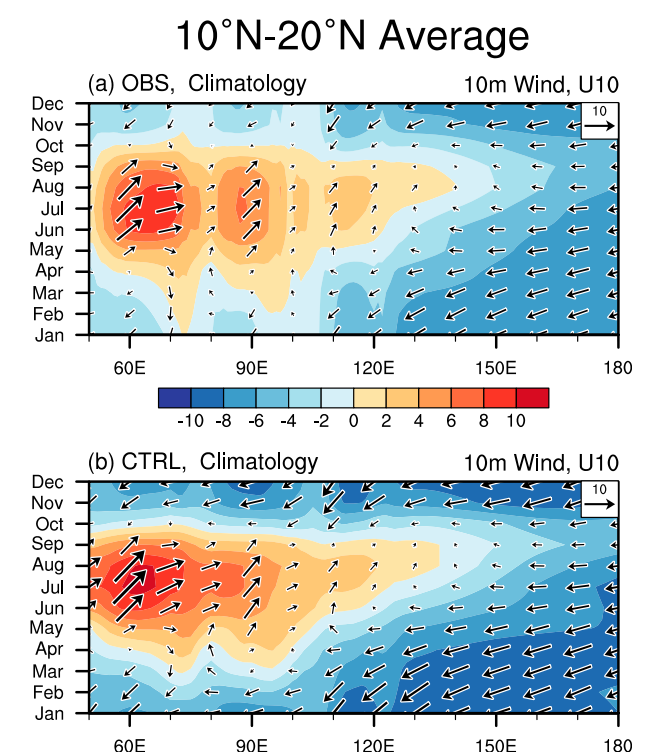


FIG. 4. The climatology of (a),(b) rainfall, horizontal wind at 925 hPa, and (c),(d) SST during June in the (top) observations and (bottom) CESM CTRL run. The climatologies in the observations and CESM CTRL run are computed during the periods of 1982–2019 and 251–300, respectively.



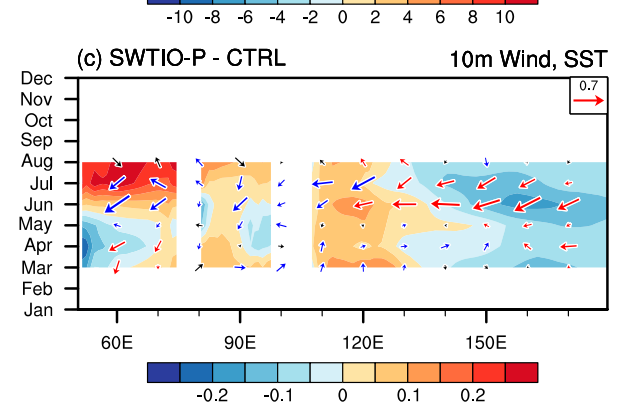


FIG. 5. Seasonal evolution of surface wind averaged over 10°–20°N (a) For the observations, (b) for the CESM CTRL run, and (c) for the differences between the SWTIO-P run and CTRL run. Red and blue arrows in (c) indicate that the corresponding mean wind speed in SWTIO-P run is greater than and less than those in CTRL run, respectively. The shading in (a) and (b) is the zonal wind speed, and the shading in (c) is SST.

to the southwest TIO warming, atmospheric circulation changes obviously over the TIO. The southwest TIO warming enhances in situ convection and induces northerly wind response across the equator (Fig. 6a). A C-shaped wind response pattern over TIO gradually forms in springtime mainly due to the Coriolis effect (Fig. 6b). From May to July, the C-shaped wind response pattern is antisymmetric along the equator with northeasterly wind response in the north and northwesterly wind response in the south (Figs. 6c,d).

Over the TIO, the CESM-simulated wind response to southwest TIO warming is quite similar to the CAM4 results, even though the intensity of the C-shaped wind response over the TIO is slightly weaker (Figs. 1 and 6). Over the WNP, the AGCM response to the southwest TIO warming is weak without an obvious anomalous anticyclonic circulation (AAC) (Fig. 1). However, in the SWTIO-P run, the southwest TIO warming induces a strong AAC over the WNP (Fig. 6).

How does the southwest TIO warming drive the winds over the WNP? Since the southwest TIO warming induces a northeasterly or easterly response in the north TIO, this wind response weakens the wind speed when the southwesterly monsoon prevails in the north TIO (Fig. 5), and thus the north TIO losses less heat and warms up (Figs. 7 and 8). Besides, it looks like the easterly wind response can expand into the WNP (Fig. 7). In early summer, as the easterly winds prevail over the WNP (Fig. 5b), and so the easterly wind response induced by the southwest TIO warming enhances the wind speed over the WNP (Figs. 5c and 8) and cools the ocean via WES feedback (Figs. 7 and 8). The easterly wind response over the WNP may be induced by the atmospheric Kelvin wave response to the southwest TIO SST warming. Figure 9 shows the differences in streamfunction and wind at 850 hPa between SWTIO-P run and CTRL run. To the east of the southwest TIO warming, the wind response features easterlies spanning from the central Indian Ocean to the Maritime Continent, with positive and negative streamfunction response north and south of the equator, respectively (Fig. 9a). Then, this pair of streamfunction responses slightly move eastward, indicative of the atmospheric Kelvin response to the southwest TIO warming (Fig. 9b). After that, anticyclonic wind anomalies form and persist in the SCS and WNP (Figs. 9b-d). Figure 10 shows the tropospheric thickness (TT) response to the southwest TIO warming; TT is defined as the geopotential height difference between 200 and 850 hPa. In April, a positive TT response appears in the TIO, featuring a Matsuno-Gill-type response (Matsuno 1966; Gill 1980). The Kelvin-Rossby wave response in the TIO is nearly symmetric along the equator. At that time, a weak low-level northerly wind response appears in the western part of TIO, and the C-shaped wind response is not quite obvious but starts to form. A wedge-like TT response in the east Indian Ocean indicates atmospheric Kelvin wave response to southwest TIO warming (Fig. 10a). In May, the wedge-like TT response extends eastward along with a lowlevel easterly wind response in the Maritime Continent. At that time, the anticyclonic wind response develops in the WNP. Then, in June, the anticyclonic wind response is welldeveloped (Figs. 10c,d). Besides, a negative TT response appears over the WNP, indicating atmospheric Rossby wave response to the SST cooling in situ. So, on one hand, the TIO warming excites atmospheric Kelvin waves propagating into the WNP (Figs. 9 and 10). The convection east of the Philippines is suppressed owing to the Kelvin wave-induced Ekman divergence mechanism (Xie et al. 2009), in favor of the development or maintenance of AAC there. On the other hand, the WNP cooling suppresses the in situ deep convection and induces an anticyclonic circulation to its west via atmospheric Rossby wave response (Figs. 7 and 10).

# The Differences between SWTIO-P run and CTRL run

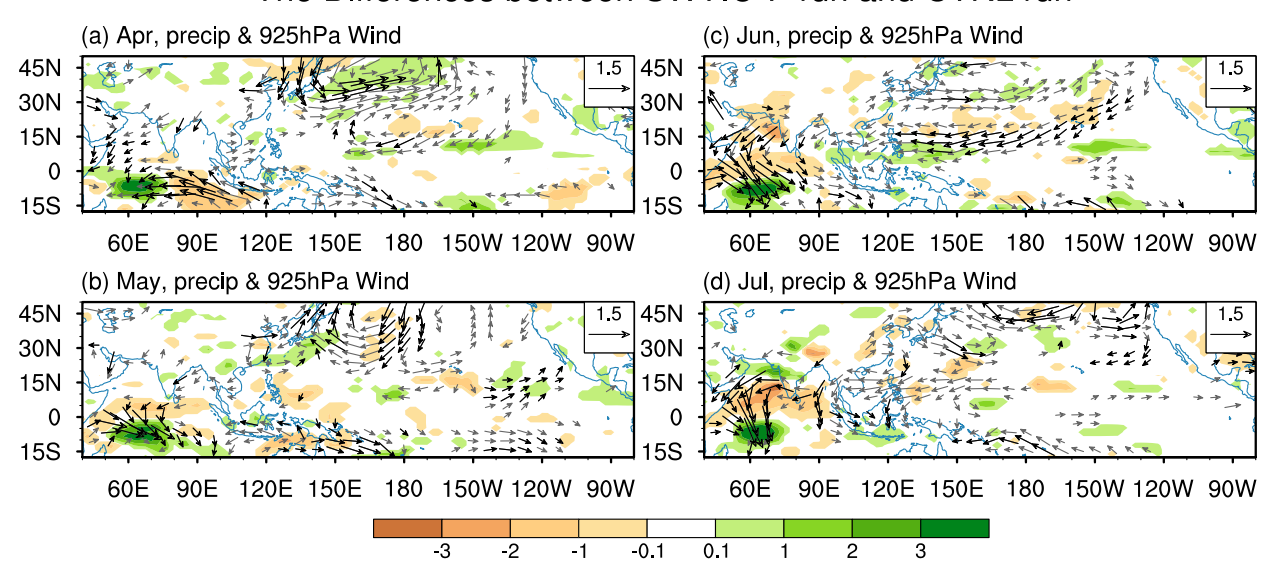


FIG. 6. The simulated rainfall (mm day<sup>-1</sup>; shading), and low-level wind (m s<sup>-1</sup>; vectors) differences between SWTIO-P run and the CTRL run. Wind differences with magnitude greater than  $0.3 \,\mathrm{m\,s^{-1}}$  are plotted. The black vectors denote that the wind response is significant at the 90% confidence level according to the Student's t test.

As the easterly wind response induces negative SST anomalies under the trade wind regime but induces positive SST anomalies in the westerly monsoon regime, due to WES feedback (Figs. 5c, 7, and 8), the seasonal variation in the background wind over the WNP changes the type of feedback (Chou et al. 2009). Our numerical results show that the southwest TIO warming induces upward and downward

motion responses in the southwest TIO and north Indian Ocean, respectively. There is a meridional circulation response across the Indian Ocean, linking the north Indian Ocean warming to the southwest TIO forcing (figures not shown). The southwest TIO warming induces a C-shaped wind response with easterly wind response in the north Indian Ocean. In May, under the background of the Asian summer

### The Differences between SWTIO-P run and CTRL run

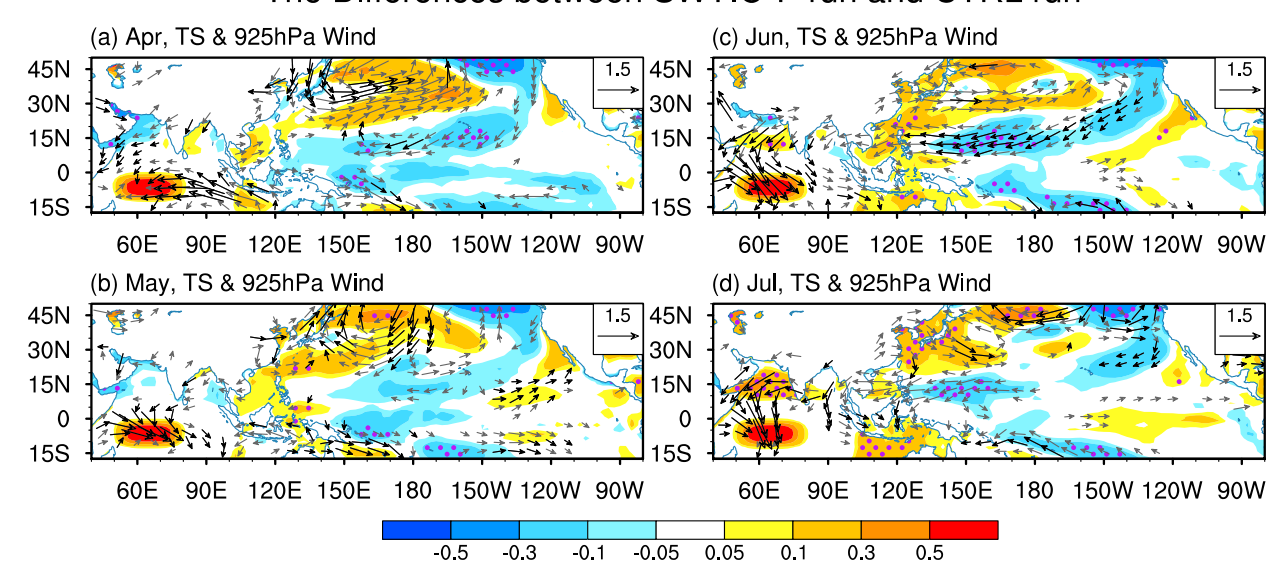


FIG. 7. As in Fig. 6, but for the results of simulated surface temperature ( $^{\circ}$ C; shading) and low-level wind [m s $^{-1}$ ; vectors (identical to those in Fig. 6)]. The stippling denotes that the surface temperature response is significant at the 90% confidence level according to the Student's t test.

# The Differences between SWTIO-P run and CTRL run

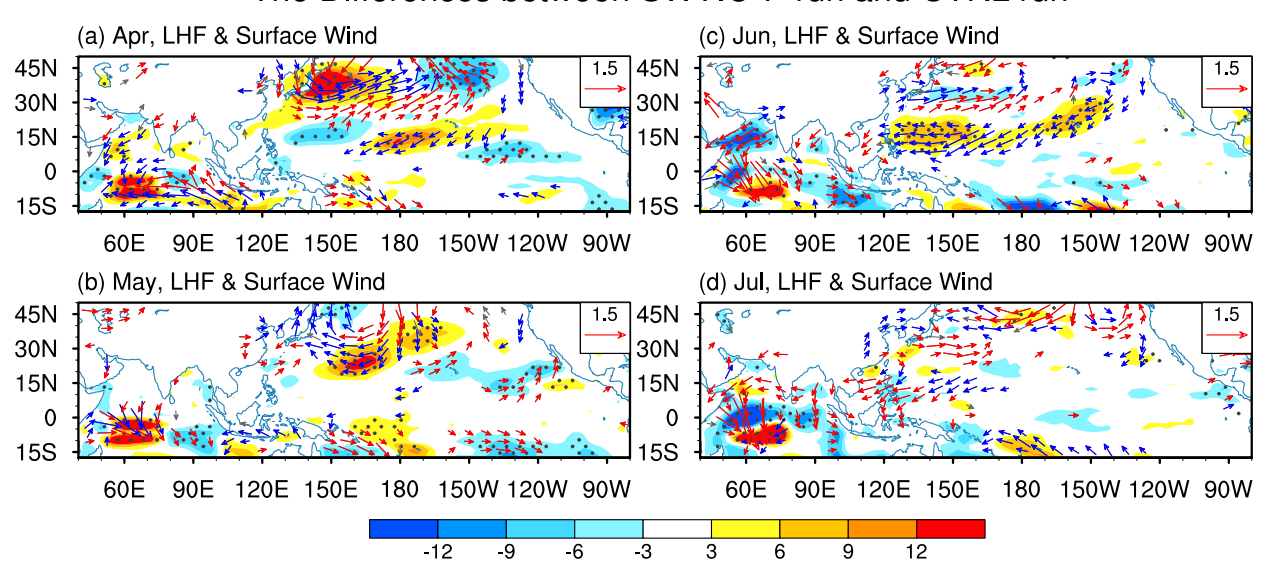


FIG. 8. As in Fig. 6, but for the results of simulated surface latent heat flux (W m $^{-2}$ ; shading) and surface wind (m s $^{-1}$ ; vectors). Red and blue arrows indicate where the wind speeds in SWTIO-P run are greater than and less than those in the CTRL run, respectively. The stippling denotes that the latent heat flux response is significant at the 90% confidence level according to the Student's t test.

monsoon, the easterly response in the north Indian Ocean induces positive WES feedback and warms the north Indian Ocean. In short, the southwest TIO could play a role in forcing the north Indian Ocean due to WES feedback. Besides, the southwest TIO warming induces atmospheric Kelvin wave response near the Maritime Continent, triggering the anticyclonic wind response over the WNP (Figs. 9 and 10). In June,

the anticyclonic wind response is well established with a significant easterly response in its southern part. At that time, the subtropical WNP is still controlled by trade winds (Fig. 5c). Thus, the easterly wind response induces positive WES feedback and cools the local SST, which in turn maintains the anticyclonic wind response. (Figs. 7c and 8c). The WNP SST cooling and TIO warming mutually contribute to the

### The Differences between SWTIO-P run and CTRL run

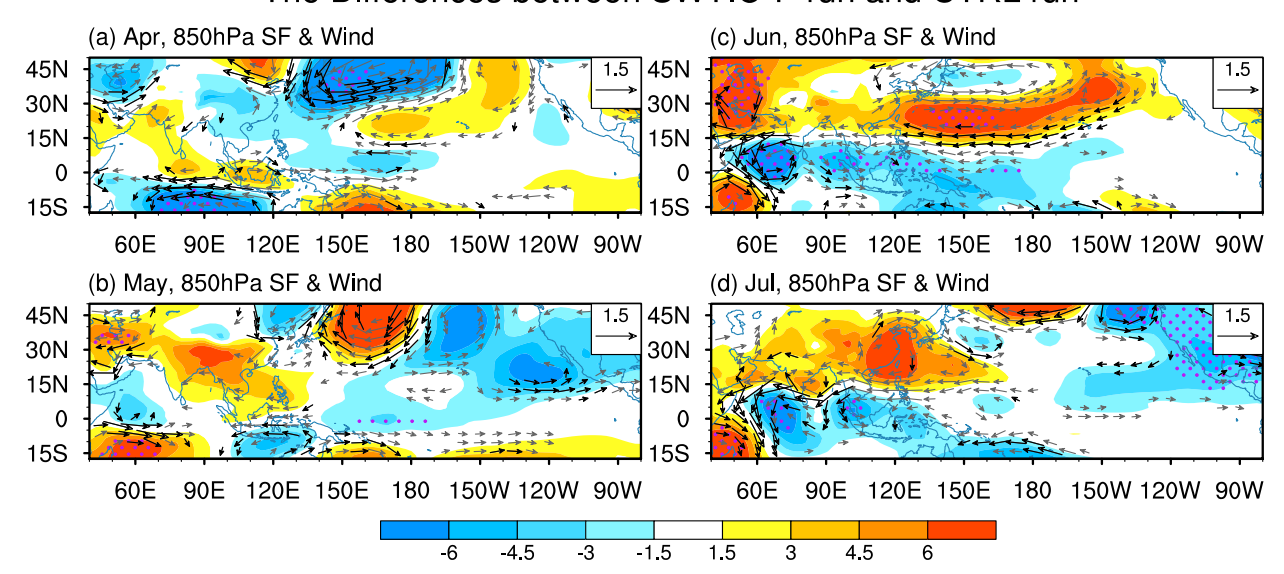


FIG. 9. The simulated streamfunction ( $m^2 s^{-1}$ ; shading) and wind ( $m s^{-1}$ ; vectors) differences at 850 hPa between the SWTIO-P run and the CTRL run. The stippling denotes that the streamfunction response is significant at the 90% confidence level according to the Student's t test.

# The Differences between SWTIO-P run and CTRL run

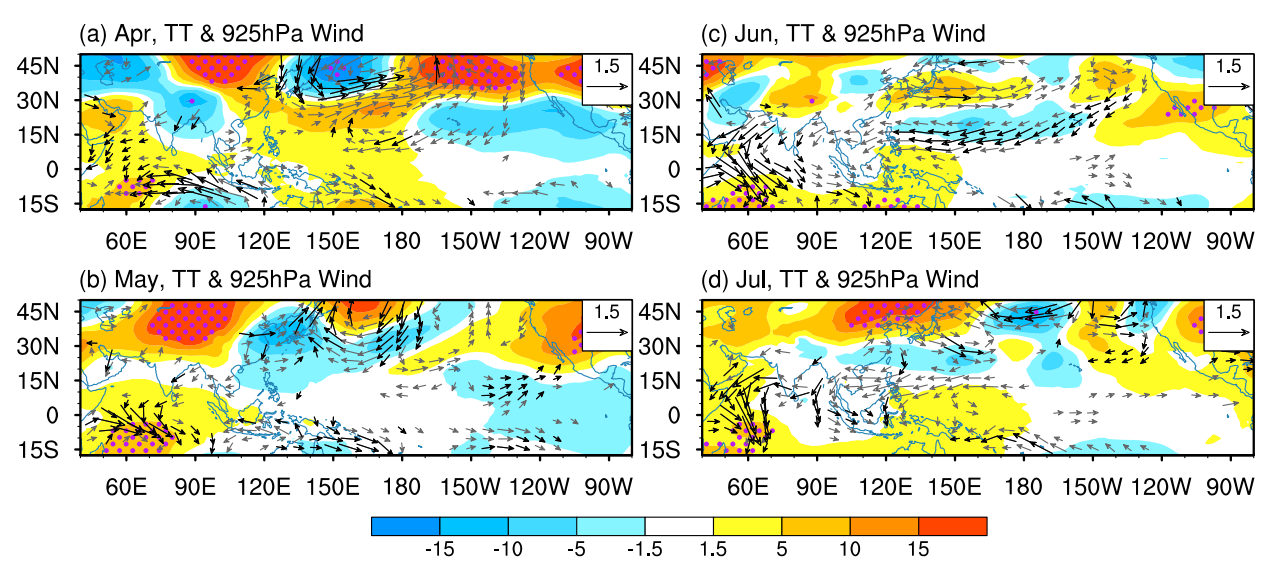


FIG. 10. As in Fig. 9, but for the results of simulated tropospheric thickness and low-level wind. The stippling denotes that the tropospheric thickness response is significant at the 90% confidence level according to the Student's *t* test.

development of ACC over the WNP (Wu et al. 2014). When the climatological winds over the WNP change from easterly to westerly (Fig. 5b), the positive WES feedback over the WNP turns negative, and thus the cold SST anomalies east of the Philippines decay (Figs. 7d and 8d).

The north TIO SST warming, WNP SST cooling, and AAC constitute an interbasin coupled mode called the Indo-western Pacific Ocean capacitor (IPOC; Xie et al. 2016). The prevailing monsoon westerlies are a necessary condition for the Indowestern Pacific interbasin coupling (Kosaka et al. 2013). In spring, an AAC and WNP SST cooling are coupled in the presence of trade winds. In summer, the AAC and north Indian Ocean warming are coupled in the Asian monsoon season as the easterly wind anomalies in the southern flank of AAC extend westward to the north Indian Ocean. IPOC is a concept combining the western North Pacific air-sea interaction (Wang et al. 2000) and the Indian Ocean capacitor effect (Xie et al. 2009). IPOC does not require ENSO forcing, but ENSO can induce initial perturbations to excite this mode, such as inducing Indian Ocean warming and WNP cooling (Kosaka et al. 2013). In our SWTIO-P experiment, we find that the southwest TIO warming can induce easterly wind response. This easterly response is well established around June, prevailing over the north Indian Ocean, SCS, and WNP. To some extent, it induces north TIO warming and WNP cooling. Thus, the southwest TIO warming could be a trigger to IPOC mode.

### 4. The role of southwest TIO warming in 2020

In June 2020, the WNP subtropical high was abnormally strong and stable, the atmospheric circulation over the WNP featured an AAC (Fig. 11). Southern China, especially the Yangtze River Valley, received more rainfall (Fig. 11). The excessive rainfall caused flooding in the Yangtze River Valley.

One intriguing feature is that there is no strong AAC over the WNP during the boreal winter of 2019 (Fig. 12b). The AAC appeared near the Philippine Sea during the boreal spring of 2020 (Fig. 12c) and reached its maximum intensity in the following summer (Fig. 12d). In the northwestern flank of the AAC, the southwesterly wind anomalies brought more moisture from the South China Sea and the north Indian Ocean into southern China, thus southern China received excessive rainfall (Fig. 12d).

El Niño can affect the East Asian climate (e.g., Huang and Sun 1992; Zhang et al. 1996; Chen 2002; Chen et al. 2017). Note that only a weak El Niño occurred in the tropical central Pacific during the previous winter. If we use Niño-3.4 index to quantify this El Niño event, its magnitude is about 0.4°C (Fig. 12b). And this weak El Niño appears like a central Pacific El Niño with its maximum positive SST anomalies located near the international date line (Fig. 12b). Previous studies have documented that the influence of central Pacific El Niño on southern China's rainfall seems weak in its decaying summer. In addition, the anticyclonic circulation in the WNP appears weak in CP El Niño decaying phase (e.g., Yuan and Yang 2012; Yuan et al. 2012). So, the strong summertime AAC in the year 2020 is quite a confusing phenomenon.

Some factors may explain why the AAC was abnormally strong in 2020, such as TIO warming (Takaya et al. 2020; Zhou et al. 2021), Atlantic warming (Zheng and Wang 2021), and high latitude wave train activity (Ding et al. 2021). Here, we highlight the trans-basin impact of the southwest TIO SST warming. The southwest TIO warming could remotely influence the Indo-Pacific atmospheric circulation and rainfall, as indicated by the regression results on the southwest TIO SST index (Fig. 2). Southwest TIO SST warming is significantly associated with a north TIO SST warming, WNP SST cooling, C-shaped wind anomalies pattern in the TIO and AAC over

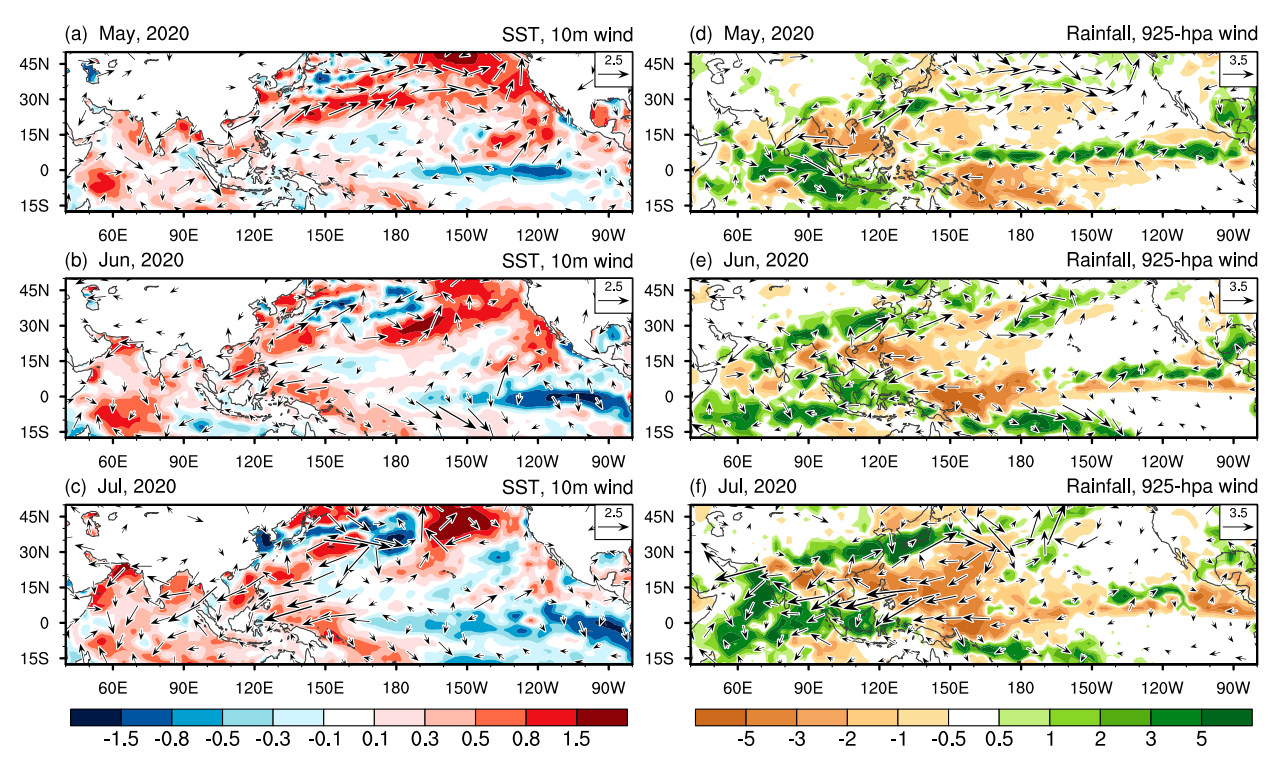


Fig. 11. SST( $^{\circ}$ C), rainfall (mm day $^{-1}$ ), and surface and low-level wind (m s $^{-1}$ ) anomalies from May to July in 2020. Wind speeds greater than 0.5 m s $^{-1}$  are plotted.

the WNP (Fig. 2). Such observational results are also confirmed by the CESM SWTIO-P run (Fig. 7). Considering the close relationship between the southwest TIO SST index and Niño-3.4 index in early boreal summer (Fig. 2a), the regressed results associated with the southwest TIO SST warming may be blurred by the simultaneous impacts of ENSO, and we may overstate the impacts of the southwest TIO warming. To remove the simultaneous impacts of ENSO, we also computed the partial regression onto the southwest TIO SST index after excluding the regressed field onto the Niño-3.4 index in May-June-July (Figs. 2c,d). The regressed signals associated with the southwest TIO warming largely disappear in the central to eastern Pacific, whereas the signals are still clear in the TIO and WNP. This suggests that the southwest TIO SST warming itself could have a significant influence on the WNP region, mainly through affecting the intensity of the AAC over the WNP (Figs. 2c,d). Note that in June 2020, the southwest TIO SST warming is abnormally strong (Fig. 11), and the atmospheric anomaly pattern over TIO and WNP resembles the SWTIO-P simulation (Figs. 6, 7, and 11). The resemblance also gives us confidence that the southwest TIO warming can remotely affect the climate over East Asia and WNP.

Studies showed that an extreme IOD event occurred during boreal autumn of 2019, the SST cooling in its eastern pole suppressed deep convection off Sumatra and Java, the Walker circulation slowed down, and anomalously strong easterly winds appeared over the equatorial Indian Ocean (e.g., Wang et al. 2020; Du et al. 2020). In the 2019 extreme IOD event, the easterlies were particularly strong along the equator, and an

anticyclonic surface wind anomaly pattern appeared in the south Indian Ocean (Fig. 10a). Such wind stress curl anomalies could induce Ekman pumping and force westward propagating oceanic Rossby waves (e.g., Huang and Kinter 2002; Xie et al. 2002; Zhou et al. 2021). This may partly explain the SST warming in the southwest TIO. It still needs more studies to quantify why there is a strong southwest TIO SST warming in early boreal summer, a topic beyond the scope of present work.

#### 5. Summary and discussion

In this study, we have revisited the role of southwest TIO SST warming in modulating the Indo-Pacific climate by using coupled model simulations. The model results show that the southwest TIO SST warming exerts a trans-basin influence on the Indo-Pacific region. In response to the southwest TIO SST warming, the local convection intensifies with an enhanced upward motion. This induces anomalous downward motion in the north TIO and low-level northerly wind response across the equator. The Coriolis force off the equator acts on this northerly wind response, resulting in a C-shaped wind response pattern with northeasterly and northwesterly wind response over the north and south TIO, respectively.

After the Asian summer monsoon onset, the southwesterly winds are established in the background over the North TIO in May, marching eastward into the WNP around July. The easterly wind response over the North TIO weakens the monsoonal winds, reduces the latent heat flux loss from the ocean, and thus warms the north TIO. In early boreal summer, the

### SST & Surface Wind Anomalies

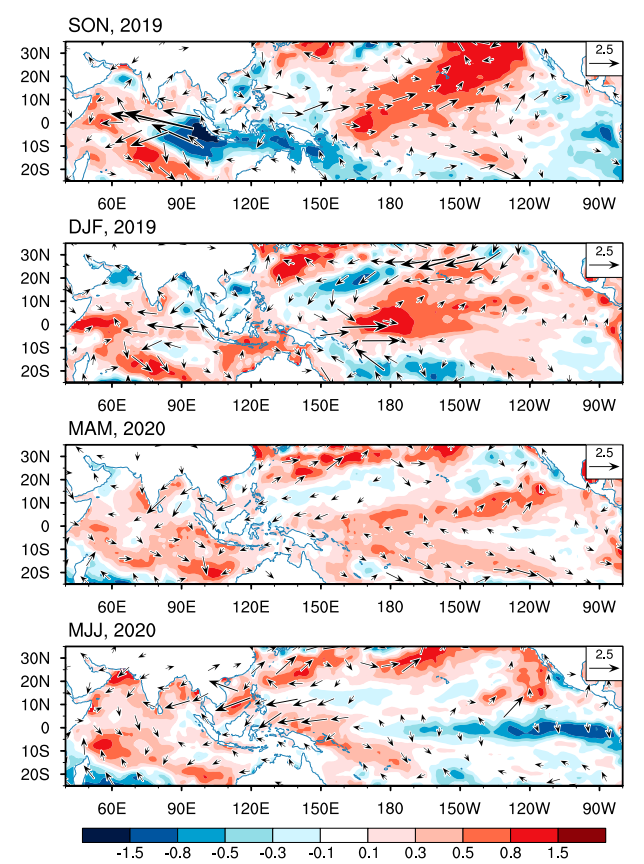


FIG. 12. SST and surface wind anomalies from boreal autumn in 2019 to summer in 2020. Wind speeds greater than  $0.5\,\mathrm{m\,s}^{-1}$  are plotted.

easterly wind response extends into the SCS and WNP. In June, the trade winds still prevail in the WNP, and so the easterly wind response in the WNP enhances local wind speed and latent heat flux loss from the ocean, and thus contributes to the SST cooling in the WNP.

In early boreal summer, both the SST warming in the TIO and SST cooling in the WNP contribute to an AAC over the east of the Philippine Sea. The TIO SST warming forces atmospheric Kelvin waves penetrating to the western Pacific, and thus induces or maintains the AAC in the WNP through the Ekman divergence mechanism (Xie et al. 2009). Besides, the WNP SST cooling suppresses the deep convection locally and is in favor of the development of the AAC through atmospheric Rossby wave response. The North TIO SST warming, WNP SST cooling, and AAC constituted an interbasin coupled mode known as IPOC. The observational regression results onto the southwest TIO SST index imply, and the CESM simulations confirm, that the southwest TIO warming could trigger the IPOC. In this paper, we focus on the trans-basin influence of the southwest TIO SST warming. In the SWTIO-P experiment, an idealized SST forcing is prescribed in the southwest TIO. This SST forcing can result from either IOD or El Niño, or both, or other external forcings. We also compared the composite results of four strong El Niño and four IOD events associated with following southwest TIO SST warming (figures not shown). Overall, they show a similar pattern, although there are some slight differences. There is no dramatic difference in the trans-basin influence of the southwest TIO warming whether it is forced by antecedent El Niño or not.

The southwest TIO warming during boreal summer is closely related to the El Niño in the previous winter. The correlation between the November (-1)-December (-1)-January (0) Niño-3.4 index and the May(0)–June(0)–July(0) southwest TIO SST index is high, reaching 0.71 (Fig. 13a). During 1982-2010, six strong El Niño events (i.e., 1982/83, 1991/92, 1997/98, 2002/2003, 2009/10, and 2015/16) are followed by the southwest TIO SST warming in the subsequent early summer. Of six years (i.e., 1983, 1987, 1991, 1998, 2015, and 2020) with strong or extreme southwest TIO SST warming during early boreal summer, four (1983, 1987, 1998, and 2015) are preceded by El Niño and two (1991 and 2020) are preceded by weak El Niño or neutral conditions (Fig. 13a). Thus, the southwest TIO warming is often related to El Niño events, but the strong southwest SST warming of early 2020 was a notable exception. The southwest TIO warming could be induced by the internal variability in the TIO. Especially, an extreme Indian Ocean dipole took place in boreal autumn of 2019. The SST cooling in the eastern Indian Ocean suppressed deep convection and slowed down the Walker circulation. The anticyclonic wind stress anomalies in the central to the eastern part of south TIO forced downwelling oceanic Rossby waves, which propagated slowly westward, deepened the thermocline, and contributed to the SST warming in the southwest TIO (e.g., Huang and Kinter 2002; Xie et al. 2002; Zhou et al. 2021). We note that four strong IOD events (i.e., 1994, 1997, 2006, and 2019) are all followed by the southwest TIO SST warming in the subsequent early summer (Fig. 13b). The correlation coefficient between the September(-1)-October(-1)-November(-1)DMI and the May(0)-June(0)-July(0) southwest TIO SST index is significant (around 0.45; Fig. 13b), supporting that the Indian Ocean dipole could modulate the SST variability in the southwest TIO.

In early boreal summer 2020, southern China suffered severe rainfall and flooding. A strong AAC over the WNP intensified the moisture transport from the tropical oceans into southern China. Unlike the El Niño-induced AAC, the summer AAC did not evolve from an AAC in wintertime. In 2020, the AAC first appeared in boreal spring and was well established in boreal summer. This AAC was associated with a TIO SST warming and WNP SST cooling from boreal spring to summer in 2020. In particular, the southwest TIO warming was strong. The observational wind and SST anomalies in early boreal summer 2020 resemble the response to southwest TIO warming in our CESM experiments. The similarity between the observations and numerical model results gives us the confidence in that the southwest TIO SST warming could have a remote influence on East Asia and the WNP climate via interbasin air-sea interaction. Our results suggest that the strong southwest TIO SST warming caused the strong AAC in the WNP during the boreal summer of 2020.

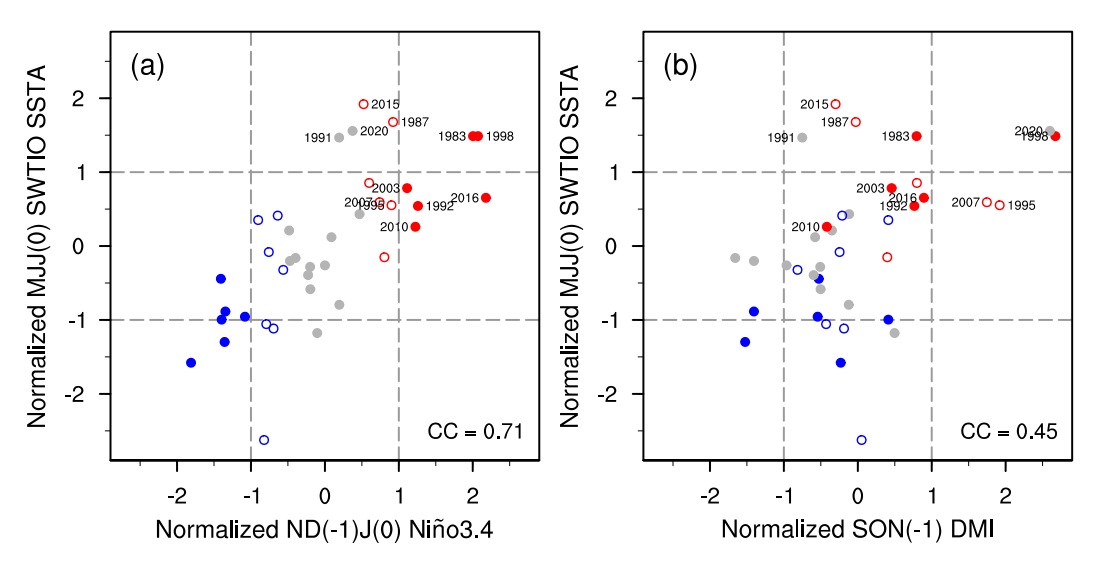


FIG. 13. (a) A scatterplot showing the correlation between the previous winter (NDJ) Niño-3.4 index and subsequent MJJ SWTIO SST index. (b) As in (a), but for previous autumn (SON) DMI index and MJJ SWTIO SST index. SON(-1), ND(-1)J(0), and MJJ(0) stand for September(-1)-November(-1), November(-1)-January(0), and May(0)-July(0), respectively, where numerals -1 and 0 denote the previous and current year, respectively; CC is correlation coefficient. El Niño and La Niña decaying years are marked as red and blue circles in the plot, respectively, with filled circles representing strong ENSO decaying years. We also label the years associated with strong El Niño events in the previous winter or strong IOD events in the previous winter, or strong southwest TIO warming in the early boreal summer.

This study shows that the southwest TIO SST warming could remotely modulate the atmospheric circulation over the western North Pacific. But we do not rule out the role of other regions in the TIO in modulating the atmospheric circulation over the western North Pacific. Indeed, we also find that the summer SST variability off the Sumatra is related to the change of atmospheric circulation over the WNP (Chen et al. 2018, 2019). So, it is hard to simply conclude that the southwest TIO is more effective to remotely modulate the atmospheric circulation over the WNP than any other region in the TIO. We think it depends on the specific case.

We also conducted a series of LBM experiments to show that southwest TIO heating can induce atmospheric Kelvin wave response in the Indo-Pacific region. The LBM model was run at a horizontal resolution using a T42 spectral truncation, roughly equivalent to 2.8 latitude × 2.8 longitude, with 20 vertical levels using a sigma coordinate system (Watanabe and Kimoto 2000). We use a time integration method to obtain the steady response, and the model integration is continued up to 30 days. The results of the 5-day average from day 20 to day 25 are shown as the steady response to prescribed diabatic heating. To explore the role of diabatic heating over the southwest TIO, an elliptic heat source (centered at 6.5°S, 65°E) was prescribed over the southwest TIO during the integration. The maximum heating rate is about 1.7 K day<sup>-1</sup> at 370 hPa, and it is approximately equivalent to heating associated with a rainfall of 2.5 mm day<sup>-1</sup>, which is consistent with the rainfall response in the SWTIO-P run. We also change the mean state used in the LBM model. However, the modeling results seem very similar. The TT response features a Kelvin wave response pattern. In the lower troposphere, easterly wind response appears over the north Indian Ocean and western Pacific. Even though the anticyclonic wind response over the western North Pacific is weak in comparison with the observations or SWTIO-P run (figures not shown), this study suggests that it can initiate the IPOC.

Acknowledgments. We thank three anonymous reviewers for their careful and constructive reviews. We also thank Dr. Y. Guo from Fudan University and Miss Y. Liang from South China Sea Institute of Oceanology for helping to set up the LBM experiments. This work is jointly supported by the National Key R&D Projects of China (2019YFA0606703), the Chinese Academy of Sciences (XDB42010305, ISEE2018PY06), the National Natural Science Foundation of China (42175043, 41830538, 41805057, 42090042), the Southern Marine Science and Engineering Guangdong Laboratory (Guangzhou) (GML2019ZD0303, GML2019ZD0306, 2019BT02H594), and the Independent Research Project Program of State Key Laboratory of Tropical Oceanography (LTOZZ2102). The authors acknowledge the support of the High-Performance Computing Division at the South China Sea Institute of Oceanology, Chinese Academy of Sciences, Guangzhou, China. The authors declare that they have no conflict of interest.

#### REFERENCES

Adler, R. F., and Coauthors, 2003: The version-2 Global Precipitation Climatology Project (GPCP) Monthly Precipitation Analysis (1979–present). *J. Hydrometeor.*, **4**, 1147–1167, https://doi.org/10.1175/1525-7541(2003)004<1147:TVGPCP>2.0.CO;2.

Alexander, M. A., I. Blade, M. Newman, J. R. Lanzante, N. C. Lau, and J. D. Scott, 2002: The atmospheric bridge: The influence of

- ENSO teleconnections on air–sea interaction over the global oceans. *J. Climate*, **15**, 2205–2231, https://doi.org/10.1175/1520-0442(2002)015<2205:TABTIO>2.0.CO;2.
- Annamalai, H., P. Liu, and S.-P. Xie, 2005: Southwest Indian Ocean SST variability: Its local effect and remote influence on Asian monsoons.
  J. Climate, 18, 4150–4167, https://doi.org/10.1175/JCLI3533.1.
- Behera, S. K., and T. Yamagata, 2001: Subtropical SST dipole events in the southern Indian Ocean. *Geophys. Res. Lett.*, **28**, 327–330, https://doi.org/10.1029/2000GL011451.
- Cao, J., R. Lu, J. Hu, and H. Wang, 2013: Spring Indian Ocean-western Pacific SST contrast and the East Asian summer rainfall anomaly. *Adv. Atmos. Sci.*, 30, 1560–1568, https://doi.org/10.1007/s00376-013-2298-6.
- Chen, W., 2002: Impacts of El Niño and La Niña on the cycle of the East Asian winter and summer monsoon (in Chinese). Chin. J. Atmos. Sci., 26, 595–610.
- Chen, Z., Z. Wen, R. Wu, X. Lin, and J. Wang, 2016: Relative importance of tropical SST anomalies in maintaining the western North Pacific anomalous anticyclone during El Niño to La Niña transition years. *Climate Dyn.*, 46, 1027–1041, https://doi.org/10.1007/s00382-015-2630-1.
- —, —, and Y. Du, 2017: Roles of tropical SST anomalies in modulating the western North Pacific anomalous cyclone during strong La Niña decaying years. *Climate Dyn.*, 49, 633– 647, https://doi.org/10.1007/s00382-016-3364-4.
- ——, Y. Du, Z. Wen, R. Wu, and C. Wang, 2018: Indo-Pacific climate during the decaying phase of the 2015/16 El Niño: Role of southeast tropical Indian Ocean warming. *Climate Dyn.*, 50, 4707–4719, https://doi.org/10.1007/s00382-017-3899-z.
- —, —, —, and S.-P. Xie, 2019: Evolution of south tropical Indian Ocean warming and the climatic impacts following strong El Niño events. *J. Climate*, **32**, 7329–7347, https://doi.org/10.1175/JCLI-D-18-0704.1.
- Chiang, J. C. H., and A. H. Sobel, 2002: Tropical tropospheric temperature variations caused by ENSO and their influence on the remote tropical climate. *J. Climate*, 15, 2616–2631, https://doi.org/10.1175/1520-0442(2002)015<2616:TTTVCB>2.0.CO;2.
- Chou, C., L.-F. Huang, J.-Y. Tu, L. Tseng, and Y.-C. Hsueh, 2009: El Niño impacts on precipitation in the western North Pacific— East Asian sector. *J. Climate*, 22, 2039–2057, https://doi.org/ 10.1175/2008JCLI2649.1.
- Chowdary, J. S., S.-P. Xie, J.-J. Luo, J. Hafner, S. Behera, Y. Masumoto, and T. Yamagata, 2011: Predictability of Northwest Pacific climate during summer and the role of the tropical Indian Ocean. *Climate Dyn.*, 36, 607–621, https:// doi.org/10.1007/s00382-009-0686-5.
- Ding, Y., Y. Liu, and Z.-Z. Hu, 2021: The record-breaking Meiyu in 2020 and associated atmospheric circulation and tropical SST anomalies. Adv. Atmos. Sci., in press, https://doi.org/10.1007/s00376-021-0361-2.
- Du, Y., S.-P. Xie, G. Huang, and K. Hu, 2009: Role of air–sea interaction in the long persistence of El Niño—induced North Indian Ocean warming. *J. Climate*, 22, 2023–2038, https://doi.org/10.1175/2008JCLI2590.1.
- —, L. Yang, and S.-P. Xie, 2011: Tropical Indian Ocean influence on Northwest Pacific tropical cyclones in summer following strong El Niño. J. Climate, 24, 315–322, https://doi.org/10.1175/2010JCLI3890.1.
- ——, Y. Zhang, L.-Y. Zhang, T. Tozuka, B. Ng, and W. Cai, 2020: Thermocline warming induced extreme Indian Ocean dipole in 2019. *Geophys. Res. Lett.*, 47, e2020GL090079, https://doi.org/ 10.1029/2020GL090079.
- Findlater, J., 1969: A major low-level air current near the Indian Ocean during the northern summer. *Quart. J. Roy. Meteor. Soc.*, **95**, 362–380, https://doi.org/10.1002/qj.49709540409.

- Gent, P. R., and Coauthors, 2011: The Community Climate System Model version 4. J. Climate, 24, 4973–4991, https://doi.org/ 10.1175/2011JCLI4083.1.
- Gill, A. E., 1980: Some simple solutions for heat-induced tropical circulation. *Quart. J. Roy. Meteor. Soc.*, **106**, 447–462, https:// doi.org/10.1002/qj.49710644905.
- He, Z., R. Wu, and W. Wang, 2015: Signals of the South China Sea summer rainfall variability in the Indian Ocean. *Climate Dyn.*, **46**, 3181–3195, https://doi.org/10.1007/s00382-015-2760-5.
- Hersbach, H., and Coauthors, 2020: The ERA5 global reanalysis. *Quart. J. Roy. Meteor. Soc.*, **146**, 1999–2049, https://doi.org/10.1002/qj.3803.
- Hu, K., G. Huang, and R. Huang, 2011: The impact of tropical Indian Ocean variability on summer surface air temperature in China. J. Climate, 24, 5365–5377, https://doi.org/10.1175/2011JCLI4152.1.
- Huang, B., and J. L. Kinter, 2002: Interannual variability in the tropical Indian Ocean. J. Geophys. Res., 107, 3199, https:// doi.org/10.1029/2001JC001278.
- Huang, R., and F. Sun, 1992: Impact of the tropical western Pacific on the East Asian summer monsoon. *J. Meteor. Soc. Japan*, **70**, 243–256, https://doi.org/10.2151/jmsj1965.70.1B\_243.
- Izumo, T., C. de Boyer Montégut, J.-J. Luo, S. K. Behera, S. Masson, and T. Yamagata, 2008: The role of the western Arabian Sea upwelling in Indian monsoon rainfall variability. *J. Climate*, 21, 5603–5623, https://doi.org/10.1175/2008JCL12158.1.
- Klein, S. A., B. J. Soden, and N. C. Lau, 1999: Remote sea surface temperature variations during ENSO: Evidence for a tropical atmospheric bridge. *J. Climate*, 12, 917–932, https://doi.org/ 10.1175/1520-0442(1999)012<0917:RSSTVD>2.0.CO;2.
- Kosaka, Y., S.-P. Xie, N. C. Lau, and G. A. Vecchi, 2013: Origin of seasonal predictability for summer climate over the Northwestern Pacific. *Proc. Natl. Acad. Sci. USA*, **110**, 7574–7579, https://doi.org/10.1073/pnas.1215582110.
- Lau, N. C., and M. J. Nath, 2003: Atmosphere-ocean variations in the Indo-Pacific sector during ENSO episodes. *J. Climate*, **16**, 3-20, https://doi.org/10.1175/1520-0442(2003)016<0003:AOVITI>2.0.CO;2.
- Matsuno, T., 1966: Quasi-geostrophic motions in the equatorial area. *J. Meteor. Soc. Japan*, **44**, 25–43, https://doi.org/10.2151/jmsj1965.44.1\_25.
- Murtugudde, R., J. P. McCreary, and A. J. Busalacchi, 2000: Oceanic processes associated with anomalous events in the Indian Ocean with relevance to 1997-1998. *J. Geophys. Res.*, **105**, 3295–3306, https://doi.org/10.1029/1999JC900294.
- ——, R. Seager, and P. Thoppil, 2007: Arabian Sea response to monsoon variations. *Paleoceanography*, 22, PA4217, https:// doi.org/10.1029/2007PA001467.
- Qu, X., and G. Huang, 2012: Impacts of tropical Indian Ocean SST on the meridional displacement of East Asian jet in boreal summer. *Int. J. Climatol.*, 32, 2073–2080, https://doi.org/ 10.1002/joc.2378.
- Reynolds, R. W., N. A. Rayner, T. M. Smith, D. C. Stokes, and W. Wang, 2002: An improved in situ and satellite SST analysis for climate. *J. Climate*, **15**, 1609–1625, https://doi.org/10.1175/1520-0442(2002)015<1609:AIISAS>2.0.CO;2.
- Saji, N. H., B. N. Goswami, P. N. Vinayachandran, and T. Yamagata, 1999: A dipole mode in the tropical Indian Ocean. Nature, 401, 360–363, https://doi.org/10.1038/43854.
- Schott, F. A., S. P. Xie, and J. P. McCreary, 2009: Indian Ocean circulation and climate variability. *Rev. Geophys.*, 47, RG1002, https://doi.org/10.1029/2007RG000245.
- Takaya, Y., I. Ishikawa, C. Kobayashi, H. Endo, and T. Ose, 2020: Enhanced meiyu-baiu rainfall in early summer

- 2020: Aftermath of the 2019 super IOD event. *Geophys. Res. Lett.*, **47**, e2020GL090671, https://doi.org/10.1029/2020GL090671.
- Taylor, K. E., 2001: Summarizing multiple aspects of model performance in a single diagram. J. Geophys. Res., 106, 7183–7192, https://doi.org/10.1029/2000JD900719.
- Wang, B., R. Wu, and X. Fu, 2000: Pacific-East Asian teleconnection: How does ENSO affect East Asian climate?
  J. Climate, 13, 1517–1536, https://doi.org/10.1175/1520-0442(2000)013<1517:PEATHD>2.0.CO;2.
- Wang, G., W. Cai, K. Yang, A. Santoso, and T. Yamagata, 2020: A unique feature of the 2019 extreme positive Indian Ocean dipole event. *Geophys. Res. Lett.*, 47, e2020GL088615, https:// doi.org/10.1029/2020GL088615.
- Watanabe, M., and M. Kimoto, 2000: Atmosphere–ocean thermal coupling in the North Atlantic: A positive feedback. *Quart. J. Roy. Meteor. Soc.*, **126**, 3343–3369, https://doi.org/10.1002/ qj.49712657017.
- Wu, B., T. Li, and T. Zhou, 2010: Relative contributions of the Indian Ocean and local SST anomalies to the maintenance of the western North Pacific anomalous anticyclone during the El Niño decaying summer. *J. Climate*, 23, 2974–2986, https:// doi.org/10.1175/2010JCLI3300.1.
- Wu, R., and S. W. Yeh, 2010: A further study of the tropical Indian Ocean asymmetric mode in boreal spring. *J. Geophys. Res.*, 115, D08101, https://doi.org/10.1029/2009JD012999.
- —, B. P. Kirtman, and V. Krishnamurthy, 2008: An asymmetric mode of tropical Indian Ocean rainfall variability in boreal spring. *J. Geophys. Res.*, 113, D05104, https://doi.org/10.1029/ 2007JD009316.
- —, G. Huang, Z. Du, and K. Hu, 2014: Cross-season relation of the South China Sea precipitation variability between winter and summer. *Climate Dyn.*, 43, 193–207, https://doi.org/10.1007/ s00382-013-1820-y.
- Xie, S.-P., 1996: Westward propagation of latitudinal asymmetry in a coupled ocean–atmosphere model. *J. Atmos. Sci.*, 53, 3236–3250, https://doi.org/10.1175/1520-0469(1996)053<3236: WPOLAI>2.0.CO;2.
- ——, and S. G. H. Philander, 1994: A coupled ocean-atmosphere model of relevance to the ITCZ in the eastern Pacific. *Tellus*, 46A, 340–350, https://doi.org/10.3402/tellusa.v46i4.15484.

- —, H. Annamalai, F. A. Schott, and J. P. McCreary, 2002: Structure and mechanisms of South Indian Ocean climate variability. J. Climate, 15, 864–878, https://doi.org/10.1175/ 1520-0442(2002)015<0864:SAMOSI>2.0.CO:2.
- ——, K. Hu, J. Hafner, H. Tokinaga, Y. Du, G. Huang, and T. Sampe, 2009: Indian Ocean capacitor effect on Indo-western Pacific climate during the summer following El Niño. *J. Climate*, 22, 730–747, https://doi.org/10.1175/2008JCL12544.1.
- ——, Y. Kosaka, Y. Du, K. Hu, J. Chowdary, and G. Huang, 2016: Indo-western Pacific Ocean capacitor and coherent climate anomalies in post-ENSO summer: A review. Adv. Atmos. Sci., 33, 411–432, https://doi.org/10.1007/s00376-015-5192-6.
- Yang, J., Q. Liu, S.-P. Xie, Z. Liu, and L. Wu, 2007: Impact of the Indian Ocean SST basin mode on the Asian summer monsoon. *Geophys. Res. Lett.*, 34, L02708, https://doi.org/ 10.1029/2006GL028571.
- Yuan, Y., and S. Yang, 2012: Impacts of different types of El Niño on the East Asian climate: Focus on ENSO cycles. *J. Climate*, 25, 7702–7722, https://doi.org/10.1175/JCLI-D-11-00576.1.
- ——, and Z. Zhang, 2012: Different evolutions of the Philippine Sea anticyclone between the eastern and central Pacific El Niño: Possible effects of Indian Ocean SST. J. Climate, 25, 7867–7883, https://doi.org/10.1175/JCLI-D-12-00004.1.
- Zhan, R., Y. Wang, and X. Lei, 2011: Contributions of ENSO and east Indian Ocean SSTA to the interannual variability of northwest Pacific tropical cyclone frequency. *J. Climate*, 24, 509–521, https://doi.org/10.1175/2010JCLI3808.1.
- Zhang, R., A. Sumi, and M. Kimoto, 1996: Impact of El Niño on the East Asian monsoon: A diagnostic study of the '86/87 and '91/ 92 events. J. Meteor. Soc. Japan, 74, 49–62, https://doi.org/ 10.2151/jmsj1965.74.1\_49.
- Zheng, J., and C. Wang, 2021: Influences of three oceans on record-breaking rainfall over the Yangtze River Valley in June 2020. *Sci. China Earth Sci.*, **64**, 1607–1618, https://doi.org/10.1007/s11430-020-9758-9.
- Zhou, Z., S.-P. Xie, and R. Zhang, 2021: Historic Yangtze flooding of 2020 tied to extreme Indian Ocean conditions. *Proc. Natl. Acad. Sci. USA*, **118**, e2022255118, https://doi.org/10.1073/pnas.2022255118.